Modeling and Estimation of Self-Phoretic Magnetic Janus Microrobot With Uncontrollable Inputs

David Folio, Antoine Ferreira

Modeling and Estimation of Self-Phoretic Magnetic Janus Microrobot with Uncontrollable Inputs

David Folio and Antoine Ferreira

***Abstract*—This study theoretically investigates the modeling of spherical catalytic self-phoretic magnetic Janus microrobot (MJR) evolving in uniform viscous flow. A two-dimensional (2D) state-space representation of the MJR is developed, exhibiting a state-dependent-coefficient (SDC) form. To evaluate the consistency of the modeling formalism, a dual Kalman filter (DFK) methodology is employed with respect to experimental results when unknown parameters or uncontrollable inputs are considered. Actually, the self-phoretic thrust mechanism and the magnetodynamics of the MJR are not well-known. SDC-DKF is implemented, and we find that there is good agreement between the dynamics computed from our theoretical predictions and the experimental observations in a wide range of model parameter variations.**

***Index Terms*—Janus particle, magnetic microrobot, modeling, state-space representation, dual Kalman filtering**

I. INTRODUCTION

SELF-propelled micro/nanorobots have demonstrated their effectiveness for various tasks at the microscale [1]. They are a promising nanotechnology for different applications such as micromanipulation, biomedical or environmental remediation [2, 3]. Among proposed designs, one of the most attractive is spherical catalytic nanomotor, also referred as Janus particle (JP) [4–6]. The advantages of spherical JP microrobot are: i) the ease of their manufacturing; ii) their cheap production; iii) they can be fuctionalized; and iv) they have simple geometry, where analytical models are easily carried out. In particular, JPs have been reported to achieve self-propulsion [4–10]. Classically, a JP of radius r is composed by catalytic (e.g. Pt or enzyme-triggered) and non-catalytic components, denoted as C and N respectively. Fig.1 shows a scheme of such JP, where a chemical reaction occurs on the C region that convert a fuel A in its vicinity. This catalytic reaction ensures self-propulsion of the JP, but still remains only partially understood. Studies have identified precursory mechanisms of the propulsion: an asymmetric gradient field, ∇f, arises between the two parts N and C that self-propels the JP. The JP could be driven by bubble propulsion mechanism [4]; but without obvious bubble generation self-phoretic propulsion is basically assumed (e.g. with radius $r < 5\,\mu\text{m}$) [5, 7, 8]. Furthermore, the propulsion of JP is strongly influenced by Brownian diffusion, e.g. due to thermal or steric forces [4]. The understanding of the dynamic behavior of JP still remains challenging, especially to develop more advanced and precise microrobotics tasks [1, 6]. A first issue is to deal with the rotational diffusion which constantly reorient the JP. A basic solution is to design JP with magnetic layers together with the catalytic layers. In such case their guidance is achieved by applying an external magnetic field [5, 6, 10–13], and then the JP becomes a magnetic Janus microrobot (MJR). Literature proposes numerous examples of microrobotic system solely actuated by magnetic fields [14], e.g. with broad biomedical applications [15]. Combining magnetic guidance with catalytically powered microrobots give rise to efficient control [5, 6]. Although reliable dynamic models are already known for magnetic microrobots [14, 15], there are only limited research works on the explicit modeling and control of MJR [6, 9, 11, 13].

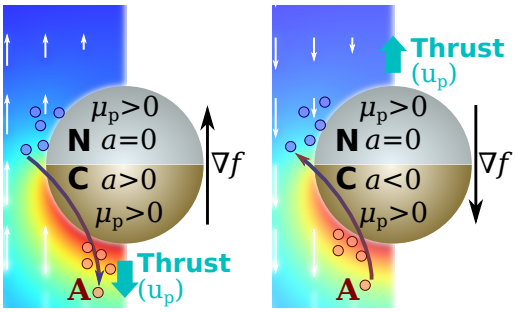

Fig. 1. Representation of Janus particle with catalytic (C) and non-catalytic (N) parts: a scheme of the catalytic reaction with, here, an homogeneous phoretic mobility μ_p, and a surface activity in the C region that (a) $a > 0$ is producing A and (b) $a < 0$ is consuming A, that induces a gradient field, ∇f, leading to a net swimming velocity, $\mathbf{u}_\text{p}$;

Actually, to define robust and predictable navigation strategies for more advanced tasks at the microscale, the explicit understanding of the MJR behavior is of prime importance for implementation of advanced control strategy. Ideally, to enable reliable biomedical applications, the controller should be robust against thermal fluctuations, weak non-uniform magnetic fields, complex shear flows... Previous works [6, 16] have considered simple Proportional-Integral-Derivative control scheme of MJR. An optimal feedback-based particle guiding method with active steering is proposed in [17]. A switching controller alternates active Brownian motion and rotation at time intervals using an optimal feedback control algorithm. The main limitation of the feedback control loop is that a numerical estimation of the Peclet number should be calculated in real-time which is cumbersome for precise localization. Model-based controllers are preferred considering their robustness and stability performance against uncertain model parameters, environmental disturbances and Brownian noise at the micro/nano-scale. In [18, 19], a kinematic model based feedback control was created based on data fitting of experimental data. However, the controller was unable

D. Folio and A. Ferreira are with INSA-CVL, Univ. Orléans, PRISME, EA 4229, Bourges, France. Corresponding authors: David Folio (e-mails: antoine.ferreira@insa-cvl.fr; david.folio@insa-cvl.fr)

Digital Object Identifier 10.1109/TCST.2021.3139192

to yield satisfactory MJR performance due to uncertainties from environmental factors. More advanced stochastic models subjected to uncertainties from environmental factors have been proposed as a solution [20]. However, such models have proved to be limited when MJRs are swimming in non-Newtonian fluids. These works demonstrate that the proposed models are not well adapted to the nonlinear multivariable motion of MJRs.

The main goal of the present work is to set out the model of MJR evolving in viscous fluids and to assess its consistency. We do not intend to focus on the self-phoretic motion, but rather aims to address the global behavior of MJRs through a continuum analysis, with a slight focus on future biomedical applications. Thus, we study the understanding of the behavior of MJR by analyzing data collected from the literature [5, 10]. Our goal is then twofold: i) to develop an adequate model that properly describes the behavior of MJR; and ii) to evaluate the proposed model according to experimental observations in order to estimate some unknown parameters or uncontrollable inputs. Indeed, common experiments with MJR mainly use magnets without well-known properties (e.g. the field and materials) which is important to characterize and control them properly [5, 6, 10, 12, 13]. Furthermore, such design parameters can vary significantly from one MJR to another. Especially, from the collected data [5, 10] used to evaluate our methodology, the magnetodynamics are not precisely known. In addition, the self-phoretic thrust mechanism is only partially understood and is subjected to Brownian diffusion. Consequently, the system inputs are not fully known or even uncontrollable. Such estimation problem is one of the most important issues in control theory. Different methodologies could be envisaged, such as considering the observer designs [21] or the Bayesian frameworks [22]. Among them, those founded on the Kalman Filter (KF) seems more relevant because they are simple to implement and use on basic Gaussian process frameworks [23–26].

To achieve these objectives, the paper is organized as follows. First, Section II presents the theoretical background which leads to a two-dimensional (2D) state-space representation of the MJR. In Section III, we propose a state dependent coefficient (SDC) with dual Kalman filter (DKF) for state and uncontrollable inputs estimation for the MJR's "pseudo-linear" system. To evaluate the consistency of the modeling, SDC-DKF algorithm is employed wrt. collected data given in [5, 10] and their supporting information (SI). The results demonstrate the consistency of the overall proposed approach when comparing experimental and estimated results.

II. THEORETICAL FOUNDATIONS

A. Catalytic Magnetic Janus Microrobot Modeling

The motion of a magnetic Janus microrobot in a viscous fluid is described by the following basic Newtonian dynamics expressed in the workspace reference frame $\{O : x_0, y_0, z_0\}$:

$$\begin{cases} M\dot{\mathbf{v}} &= \mathbf{f}_\mathrm{p} + \mathbf{f}_\mathrm{d} + \mathbf{f}_\mathrm{ext} + \mathbf{f}_\mathrm{a} \\ J\dot{\boldsymbol{\omega}} &= \mathbf{t}_\mathrm{p} + \mathbf{t}_\mathrm{d} + \mathbf{t}_\mathrm{ext} + \mathbf{t}_\mathrm{a} \end{cases} \tag{1}$$

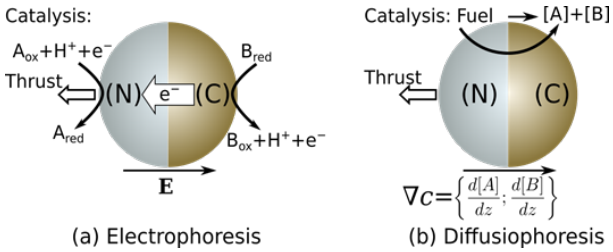

Fig. 2. Self-phoretic propulsion: (a) self-diffusiophoretic driven by catalytic reaction of the decomposition of the fuel from the surrounding medium as a result of concentration gradient of species: ∇c; (b) self-electrophoresis from catalytic redox reaction of active MJR capable of generating its own dynamic electric field, E. The both propulsion mechanisms are able to induce a self-thrust motion.

where M and J are the mass and the moment of inertia of the MJR; $\mathbf{v}$ and $\boldsymbol{\omega}$ are its linear and angular velocities; $\mathbf{f}_\mathrm{p}$ and $\mathbf{t}_\mathrm{p}$ are related to the self-propulsion mechanism; $\mathbf{f}_\mathrm{d}$ and $\mathbf{t}_\mathrm{d}$ denote the hydrodynamic drag force and torque; $\mathbf{f}_\mathrm{ext}$ and $\mathbf{t}_\mathrm{ext}$ are the other external forces and torques; $\mathbf{f}_\mathrm{a}$ and $\mathbf{t}_\mathrm{a}$ are the external action or controlled force and torque. Fig. II-A4 depicts the relevant forces and coordinate systems. The following paragraphs describe the relevant modeling parts given in Eq. (1).

1) Self-propelled Spherical Janus Micromotor : Basically, catalytic MJR draw their fuel A, such as water, hydrogen peroxide (H_2O_2), urea, glucose and so on to convert it in a thrust mechanism with swimming velocity, $\mathbf{u}_\mathrm{p}$. For all such catalytic MJRs, their self-propulsion is ensured with no external energy supply. It is admitted that self-propelled MJR is set into motion due to the imbalance of phoretic effects (e.g. electrophorectic and diffusiophoretic) within the solid/liquid interfacial structure at its surface that cause a net fluid motion around it [7, 27, 28]. The resulting flow is most conveniently described by an effective slip velocity of the liquid past the solid, defined by [7, 27]:

$$\mathbf{u}_f(\mathbf{r}) = \mu_p(\mathbf{r})\,(\mathbb{I} - \mathbf{nn}) \cdot \nabla f(\mathbf{r}) \tag{2}$$

where $\mathbf{n}$ is the local normal to the surface, $\mathbb{I}$ is the identity tensor, and $\mu_p(\mathbf{r})$ is the local "phoretic mobility". $\nabla f(\mathbf{r})$ refers to the main phoretic effect, that is:

a) Diffusiophoresis: We note $\nabla f = \nabla c$ for diffusiophoresis when there are concentration gradients, of chemical species around the MJR [7, 27], as depicted in Fig. 2.b. The slip velocity is then usually expressed as [8]:

$$\mathbf{u}_{f_\mathbf{dp}} = \mu_{dp}(\zeta_p)\nabla c, \tag{3}$$

where $\mu_{dp}(\zeta_p)$ is known as the "diffusiophoretic mobility". This phoretic mobility expression differs depending on whether an ionic or non-ionic solute is considered.

b) Electrophoresis: Similarly, when there are concentration gradients $\nabla f = \nabla \Phi = \mathbf{E}$ of chemical species around the MJR, the electrophoresis occurs when the MJR is subject to a gradient of electric potential [27, 28], as depicted by Fig. 2.a. This effect leads to the well-known Helmholtz-Smoluchowski equation [8]:

$$\mathbf{u}_{f_\mathbf{ep}} = \mu_{ep}(\zeta_p)E, \tag{4}$$

where $\mu_{ep}(\zeta_p)$is referred as the "electrophoretic mobility", that is related to the zeta-potential, ζ_p, of the particle.

When both electrophoresis and difffusiophoresis are observed, the net effective slip velocity is the superposition of the two phenomena:

$$\mathbf{u}_f = \mathbf{u}_{f_{\mathbf{ep}}} + \mathbf{u}_{f_{\mathbf{dp}}}. \tag{5}$$

Let us also notice, that in some cases thermophoresis effect could also contribute in the self-phoretic propulsion. However, such thermal aspect is out of the scope of the present work, and could usually be neglected.

Next, the slip flow, $\mathbf{u}_f$, around the MJR is used to deduce its swimming velocity, $\mathbf{u}_\mathrm{p}$. Golestanian et al. [7] express the relation between the slip motion, $\mathbf{u}_f$, on a sphere of radius r to its net velocity, $\mathbf{u}_\mathrm{p}$, with the following relation over the MJR's active surface S:

$$\mathbf{u}_\mathrm{p} = -\frac{1}{4\pi r^2} \iint_S d\mathbf{r}\ \mathbf{u}_f(\mathbf{r}) \tag{6}$$

2) Hydrodynamics of Spherical Particles: Classically, the hydrodynamic behavior of a rigid body is modeled using the Navier-Stokes equations. Assuming that the steady viscous fluid is incompressible with low Reynolds number, the drag force, $\mathbf{f}_\mathrm{d}$, and torque, $\mathbf{t}_\mathrm{d}$, on a spherical MJR of radius r is basically expressed as follows:

$$\mathbf{f}_\mathrm{d} = -6\pi\eta r\ \mathbf{v} = -d_f\ \mathbf{v} \tag{7}$$

$$\mathbf{t}_\mathrm{d} = -8\pi\eta r^3\ \boldsymbol{\omega} = -d_t\ \boldsymbol{\omega} \tag{8}$$

where η is the dynamic viscosity of the fluid medium.

Without the others forces, and with the sole swimming velocity $\mathbf{u}_\mathrm{p}$, at equilibrium we basically get: $\mathbf{f}_\mathrm{p} + \mathbf{f}_\mathrm{d} = 0$, that is $\mathbf{f}_\mathrm{p} = d_f\ \mathbf{u}_\mathrm{p}$ [4].

3) External Disturbances: In the MJR dynamics given by Eq. (1), the external disturbance force, $\mathbf{f}_\mathrm{ext}$, and torque, $\mathbf{t}_\mathrm{ext}$, can embed any relevant nanoforces, such as van der Waals, electrostatic, steric, thermal actions and so on. In the proposed framework, the motion of a single MJR is assumed to be perturbed only by random fluctuations, that could be considered as Brownian. To model a Brownian motion the Langevin equation is commonly employed, leading to:

$$\mathbf{f}_\mathrm{ext} = {}^t\xi \tag{9}$$

$$\mathbf{t}_\mathrm{ext} = {}^r\xi \tag{10}$$

${}^t\xi$ and ${}^r\xi$ denote the stochastic force and torque due to random fluctuations. These noise terms are assumed to be white Gaussian probability distribution ($\langle {}^{t,r}\xi \rangle = 0$), with the following correlation function:

$$\left\langle {}^t\xi_i(t_1) {}^t\xi_j(t_2) \right\rangle = 2k_bT\ d_f\ \delta_{ij}(t_1 - t_2) \tag{11}$$

$$\left\langle {}^r\xi_i(t_1) {}^r\xi_j(t_2) \right\rangle = 2k_bT\ d_t\ \delta_{ij}(t_1 - t_2) \tag{12}$$

with $k_b = 1.38 \times 10^{-24}$ J/K the Boltzmann constant; T the effective absolute temperature; γ_{ij} the Kronecker delta with the subscript ij referring to the respective components, and $\langle \cdot \rangle$ denotes the noise average.

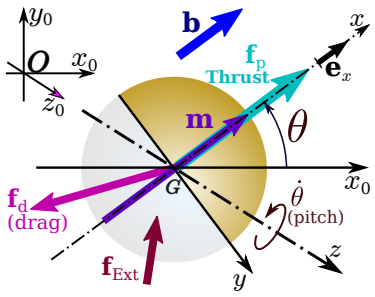

Fig. 3. Representation of forces acting on a magnetic Janus microrobot (MJR) submitted to an external applied magnetic field $\mathbf{b}$.

4) External Actuation Control: MJR driven by magnetic fields are one of the most promising approaches compared to other propulsion mechanisms [5, 6, 29]. The basic principle of magnetic actuation is to control the magnetic field $\mathbf{b}$ to induce a magnetic force and torque on the magnetized material, commonly defined by:

$$\mathbf{f}_\mathrm{a} = \mathbf{f}_\mathrm{m} = V_\mathrm{m}\,(\mathbf{m} \cdot \nabla)\,\mathbf{b} \tag{13}$$

$$\mathbf{t}_\mathrm{a} = \mathbf{t}_\mathrm{m} = V_\mathrm{m}\ (\mathbf{m} \times \mathbf{b}) \tag{14}$$

with $\mathbf{m} = (m_x, m_y, m_z)^\top$ the MJR's magnetization (A/m); $\mathbf{b} = (b_x, b_y, b_z)^\top$ is the external magnetic field (T); and V_m the volume of the magnetic material.

B. MJR Dynamics Model

1) Assumptions: The considered MJR is axisymmetric: it possesses two distinguishable hemispheres; and with no loss of generality and for the sake of simplicity, we reduce the modeling to a two-dimensional (2D) problem in the x-y plane (see Fig. 3). Therefore, the configuration of the MJR is described by $(x, y, \theta)^\top$, where (x, y) is its location and θ is the orientation of its easy axis, $\mathbf{e}_x$, as shown in Fig. 3. The motion of the MJR is obtained from the translational velocity $\mathbf{v} = (v_x, v_y, 0)^\top$ and the rotational velocity $\boldsymbol{\omega} = (0, 0, \omega_z)^\top$. This work considers that the magnetic field, $\mathbf{b}$, is used only for directional control (i.e. the magnetic gradient is negligible at least in the vicinity of the MJR) and does not affect the (self) propulsion mechanism. We consider an homogeneous particle where the magnetization vector will coincide to the thrust vector. In this context, the controlled magnetic torque Eq. (14) contains only its z-axis component, and is reduced to: $t_{mz} = V_\mathrm{m}(m_y b_x - m_x b_y)$. We also assume that the embedded magnetic material reveals a magnetic anisotropy. The magnetic moment is considered, here, always aligned along the MJR main axis, that is: $\mathbf{m} = m \cdot \mathbf{e}_x$, with $\|\mathbf{m}\| = m$.

Next, if an azimuthally symmetric MJR with a single catalytic hemisphere (see Fig. 1), with a uniform phoretic mobility, μ_p, is considered, the swimming velocity Eq.(6) can be reduced to [7]:

$$\mathbf{u}_\mathrm{p} = u_0 \cdot \mathbf{e}_x \tag{15}$$

where the stationary velocity: $u_0 \propto \mu_p a(c_A)/D$, is mainly related to the diffusion coefficient $D = k_BT/d_f$, and the "surface activity": $a(c_A) \propto c_A$, with c_A the concentration of the fuel A (see Fig. 1).

2) 2D State-Space representation: From the above assumptions, the 2D dynamic model of MJR can be expressed with the following state-space representation:

$$(S_x)\ \begin{cases} \dot{x} &= v_x \\ \dot{v}_x &= -\alpha_x v_x + \alpha_x \cos(\theta) u_0 + \xi_x \end{cases} \tag{16}$$

$$(S_y)\ \begin{cases} \dot{y} &= v_y \\ \dot{v}_y &= -\alpha_y v_y + \alpha_y \sin(\theta) u_0 + \xi_y \end{cases} \tag{17}$$

$$(S_\theta)\ \begin{cases} \dot{\theta} &= \omega \\ \dot{\omega} &= -\alpha_\omega\, \omega + \beta\left(\sin(\theta) b_x + \cos(\theta) b_y\right) + \xi_\theta \end{cases} \tag{18}$$

with $\alpha_x = \alpha_y = \frac{d_f}{M}$, $\alpha_\omega = \frac{d_t}{J_{zz}}$, $\beta = \frac{V_m}{J_{zz}} m$, and the inertia[1] of spherical body: $J_{zz} = \frac{2}{5} M r^2$.

It should be noted that the inertia contribution is mainly relevant for exhibiting the transient MJR behavior. When the inertia is neglected, the dynamic model becomes then a simple kinetics model. In such a case, the translational velocity $\mathbf{v} = (v_x, v_y, 0)^\top$ and the rotational velocity $\boldsymbol{\omega} = (0, 0, \omega_z)^\top$ are no longer in the state vector. Neglecting the inertia can then be seen as a simplification of the proposed dynamic model. This can be useful for the case where the self-phoretic remains globally unchanged, or when the magnetic control is not changing too fast. But for other applications (e.g. the fuel concentration may change significantly or using soft-magnetic materials) taking into account the full dynamics may become important.

Let $\mathbf{x} = (x, v_x, y, v_y, \theta, \omega)^\top$ denotes the state vector; $\mathbf{u} = (u_0, b_x, b_y)^\top$ defines the control inputs; $\mathbf{y} = (x, y, \theta)^\top$ is the measured outputs; and $\boldsymbol{\xi} = (0, \xi_x, 0, \xi_y, 0, \xi_\theta)^\top$ is a white Gaussian noise computed from the Brownian motion. The 2D state-space representation of the system can be rewritten as:

$$\dot{\mathbf{x}} = \mathbf{A}\,\mathbf{x} + \mathbf{B}(\mathbf{x})\,\mathbf{u} + \boldsymbol{\xi} \tag{19}$$

$$\mathbf{y} = \mathbf{C}\mathbf{x} + \boldsymbol{v} \tag{20}$$

where the system matrices are defined by:

$$\mathbf{A} = \mathrm{diag}\left[\begin{pmatrix} 0 & 1 \\ 0 & -\alpha_x \end{pmatrix}, \begin{pmatrix} 0 & 1 \\ 0 & -\alpha_y \end{pmatrix}, \begin{pmatrix} 0 & 1 \\ 0 & -\alpha_\omega \end{pmatrix}\right] \tag{21}$$

$$\mathbf{B}(\mathbf{x}) = \begin{pmatrix} 0 & 0 & 0 \\ \alpha_x \cos(\theta) & 0 & 0 \\ 0 & 0 & 0 \\ \alpha_y \sin(\theta) & 0 & 0 \\ 0 & 0 & 0 \\ 0 & \beta \sin(\theta) & \beta \cos(\theta) \end{pmatrix} \tag{22}$$

$$\mathbf{C} = \mathrm{diag}\left[\begin{pmatrix} 1 & 0 \end{pmatrix}, \begin{pmatrix} 1 & 0 \end{pmatrix}, \begin{pmatrix} 1 & 0 \end{pmatrix}\right] \tag{23}$$

and $\boldsymbol{v} \sim \mathcal{N}(0, \mathbf{R})$ is the observation noise which is assumed to be zero mean Gaussian white noise with covariance matrix $\mathbf{R}$.

3) System Analysis: The MJR model (16)-(18) may at first glance appears as a nonlinear system. Specifically, its dynamics is represented by a linear structure (19)-(20) having state-dependent coefficient (SDC) form, and it is then said "pseudo-linear". Basically, SDC parametrization is not unique, and must be chosen wrt. the system and control objective [30]. A first key issue is to analyze the property of the SDC parametrization. Recalling that KF is used to evaluate the modeling suitableness, the *SDC observability matrix*, $\mathcal{O}(\mathbf{x})$, has to be investigated. As in the linear theory, the matrix is defined as:

$$\mathcal{O}(\mathbf{x}) \triangleq \begin{bmatrix} \mathbf{C} & \mathbf{CA} & \mathbf{CA}^2 & \dots & \mathbf{CA}^5 \end{bmatrix}^\top \tag{24}$$

If $\mathcal{O}(\mathbf{x})$ has full rank (i.e. $\mathrm{rank}\{\mathcal{O}(\mathbf{x})\} = 6$) for the entire domain for which the system is to be observed then the system is observable [30]. It can be shown that the considered pseudo-linear system (19)-(20) is fully observable $\forall \mathbf{x} \in \mathbb{R}^6$.

[1] In most cases, at low Reynolds number the inertia effects can be neglected. But to get the velocities and the transient behaviors, it should be kept in the model.

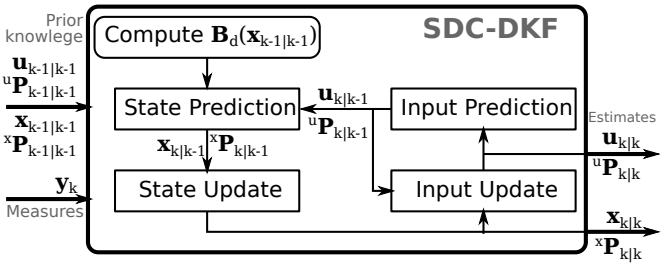

Fig. 4. Scheme of the SDC-DKF algorithm: the prediction and update steps are based on common KF formalism.

C. Kalman Filter for State and Input Estimations

To evaluate the consistency of the proposed model wrt. experiments, Kalman filtering (KF) approach is envisaged. As stated, the control inputs, $\mathbf{u}$, are assumed unknown and have to be estimated. Indeed, we consider here that the magnetic field, $\mathbf{b}$, and the stationary thrust, u_0, are not available or not well-known. Literature reports different methods to cope with the lack of such information [21–26, 31]. The KF is chosen for its simplicity of implementation and its ability to deal with stochastic systems. Based on this framework, two strategies are commonly considered for parameters or uncontrollable inputs estimation issue: build an augmented Kalman filter (AKF) which embed both the states, $\mathbf{x}$, and the unknown parameters or uncontrollable inputs [25]; or use a dual Kalman filter (DKF) [23]. However, the AKF is known to be prone to numerical instabilities due to unobservability issues of the augmented system matrix [25]. In contrast, the DKF outperforms the AKF at the cost of a more complex implementation [26]. Furthermore, recalling that the MJR's dynamics belongs to the class of "pseudo-linear" systems, SDC filtering, which is based on the state-dependent Riccati equation (SDRE), must also be treated [32, 33]. The solution of the SDRE represents the error covariance, and can be used to update the error covariance matrix similarly to common KF formulation. In this study, a modified DKF based on the SDC parametrization is used. Indeed, to the authors' knowledge, this work is a first attempt to use DKF with the SDC form, that is referred as SDC-DKF.

III. RESULTS

A. State Dependent Coefficient – Dual Kalman Filter

The proposed SDC-DKF estimator scheme is reported in Fig.4, and the detailled algorithm is given in Appendix A.

SDC-DKF is based on a dual stages DKF for state and input estimations where the system matrices are state-dependent. First, the continuous time system (19)-(20) is discretized at each time-step wrt. the sampling time of the system. As the MJR's model (16)-(18) is defined through a pseudo-linear state-space representation (19)-(20), the discretized matrices are evaluated with the state-dependent parameters. The structure chosen to manage the state dependent-terms is notably based on the similarity between the error covariance solution of the SDRE and that of the common KF.

Next, the SDC-DKF relies on the use of a common DKF algorithm to predict/update the input, $\hat{\mathbf{u}}_{k|k}$ and its covariance matrix, ${}^{u}\mathbf{P}_{k|k}$, with a fictitious process equation; and use this input estimation to predict/update the state, $\hat{\mathbf{x}}_{k|k}$ and its covariance matrix ${}^{x}\mathbf{P}_{k|k}$.

Assessment of stability of the SDC-DKF for a general pseudo-linear system representation, is still an open research problem, particularly due to the SDC parametrization. But, let us notice that for the SDRE to have solutions, the system should be observable in the pseudo-linear sense, that is if the SDC observability matrix (24) has full rank [30, 33], which is the case here. Moreover, in the MJR model (16)-(18), the orientation (θ) is the sole state-dependent term which is used to evaluate the input matrix $\mathbf{B}_{k-1}(\theta)$. This orientation is obtained from measurement data, but the filtered value from the estimated state can also be considered.

Finally, as one can see, the MJR's model (16)-(18) can be decoupled into 3 pseudo-linear subsystems (S_x), (S_y) and (S_θ). Each subsystem can be then estimated separately with the SDC-DKF. Especially, (S_θ) can be first estimated to get $\widehat{\theta}_{k|k}$ that can be used to compute the SDC-DKF for (S_x) and (S_y).

B. Applications

The proposed model and the SDC-DKF is evaluated on two MJRs developed by Baraban et al. [5] and Ma et al. [10] that are presented hereafter. The overall results are obtained by analyzing data collected by the referenced authors. Table I reports the relevant parameters provided in Baraban et al. [5] and Ma et al. [10].

1) Spheroidal Catalytic Janus Magnetic Microrobot: To validate the proposed dynamic model, this paper first considers the work carried out by Baraban et al. [5]. The authors have fabricated MJR that are based on a spherical silica (SiO_2) particle of radius $r = 2.5\,\mu\text{m}$. The sphere is capped with a sputtered layer of $2\,\text{nm}$ Pt, plus a deposited ultrathin multilayer of magnetic material $[\text{Co}(0.4\,\text{nm})\text{Pt}(0.6\,\text{nm})]_5$, and finally a $15\,\text{nm}$ Pt layer covers the whole to protect from oxidation and enables the catalytic reaction. Such common composition allows the decomposition of hydrogen peroxide fuel; and exhibits a perpendicular magnetic moment, $\mathbf{m}$, pointing out outwards to its surface. In the considered collected data, the MJR is immersed in 10 % aqueous solution of H_2O_2, leading to a mean swimming velocity of about $u_0 \approx 8\,\mu\text{m/s}$. The parameter set considered is reported in the Table I.a.

From the data provided by Baraban et al. [5], the positions (x, y) and orientations, θ, of a MJR are extracted and used as measurements data, $\mathbf{y}$. SDC-DKF is applied to track the MJR while estimating the unknown input $\hat{\mathbf{u}}$. The measured and the tracked path is shown in Fig. 5. As one can see, the SDC-DKF fits suitably the observed path. Fig. 6 presents the error between the measured output $\mathbf{y}$ and its estimation $\hat{\mathbf{y}}$. The root-mean-square error (RMSE) of the tracking for x, y and θ are $\text{RMSE}(x) = 0.52\,\mu\text{m}$, $\text{RMSE}(y) = 0.53\,\mu\text{m}$ and $\text{RMSE}(\theta) = 1.62\,\text{deg}$. It can be noticed that the proposed tracking methodology together with the developed modeling provide a reasonable estimate of the state $\hat{\mathbf{x}}$ of the MJR. Fig. 7 shows the unknown input estimation $\hat{\mathbf{u}}$. The estimated swimming velocity has a mean value of $\langle u_0 \rangle = 7.03\,\mu\text{m/s}$ and $\text{RMSE}(u_0) = 7.05\,\mu\text{m/s}$, that are consistent with the velocity of $8\,\mu\text{m/s}$ reported by Baraban et al. [5]. Let us notice that, as only normalized data on the magnetic properties of the MJR are available, βb_x and βb_y only can be estimated from the observed data. Fig. 7 depicts their normalized values. These results validate the consistency of the proposed dynamics model

TABLE I
PARAMETERS COLLECTED (A) FROM BARABAN ET AL. [5] AND (B) FROM MA ET AL. [10]

Params.	Value	Descriptions
r	$2.52\,\mu\text{m}$	MJR radius
η	$\sim 1\,\text{mPa s}$	fluid viscosity for 10wt% of H_2O_2
u_0	$\sim 8\,\mu\text{m/s}$	swimming velocity for 10wt% of H_2O_2
m	1	(normalized) magnetic moment
$\|\mathbf{h}\|$	$<800\,\text{A/m}$	magnetic field strength

SiO_2 bead ($r = 2.5\,\mu\text{m}$) + $\text{Pt}(2\,\text{nm})[\text{Co}(0.4\,\text{nm})\text{Pt}(0.6\,\text{nm})]_5\text{Pt}(15\,\text{nm})$

(a)

Params.	Value	Descriptions
r	$1.16 \pm 0.015\mu\text{m}$	MJR radius
η	$\sim 1\,\text{mPa s}$	viscosity of aqueous solution of urea
u_0	$\sim 10\,\mu\text{m/s}$	stationary swimming velocity
m	N/C	magnetic moment
$\|\mathbf{b}\|$	$\sim 100\,\text{mT}$	magnetic field

Janus hollow mesoporous particle + $\text{Fe}(10\,\text{nm})\text{Au}(3\,\text{nm})$

(b)

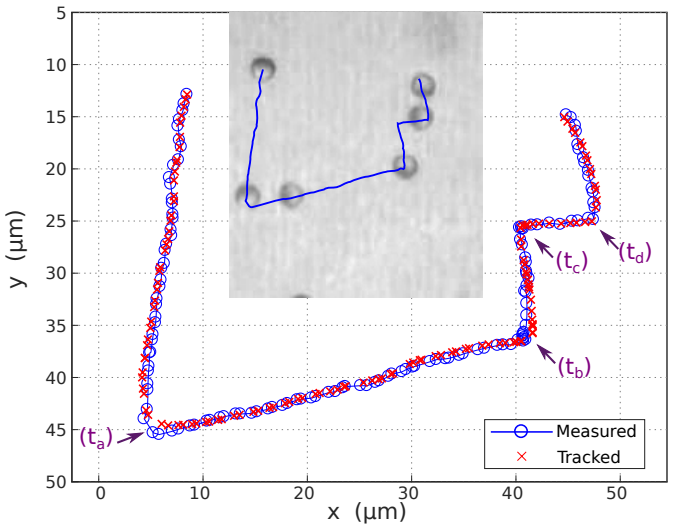

Fig. 5. Measured and tracked path of a spherical MJR using SDC-DKF, from experimental data carried by Baraban et al. [5].

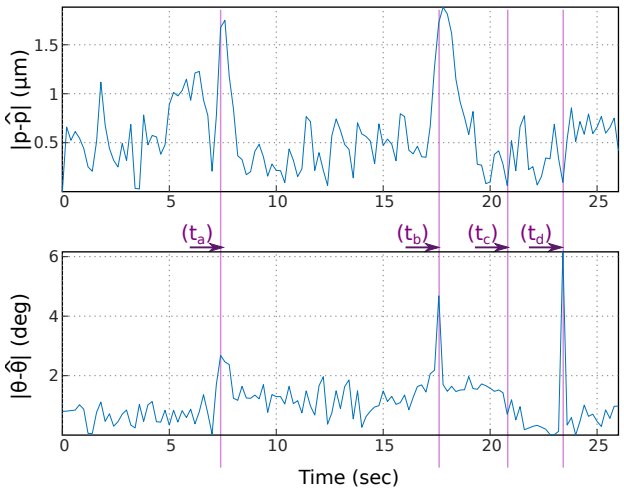

Fig. 6. The estimation error of the position ($|\mathbf{p}-\hat{\mathbf{p}}|$, with $\mathbf{p}=(x,y)$), and of the orientation, $|\theta-\hat{\theta}|$ of the spherical MJR. The t_a-t_d refer to the time when the direction is changing also annoted in Fig.5.

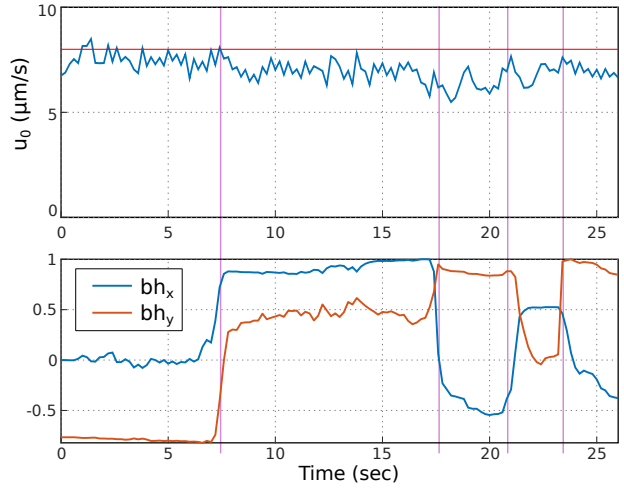

Fig. 7. The estimated input $\hat{\mathbf{u}} = (u_0, \beta b_x, \beta b_y)$ from the observed experimental data using SDC-DKF. (top) The red-line shows the mean swimming velocity of $u_0 \approx 8\,\mu\text{m/s}$ reported by Baraban et al. [5]. (bottom) normalized value of the field βb_x and βb_y.

to describe the behavior of MJR, while allowing accessing to the uncontrollable inputs.

2) Urea-powered Biocompatible Spherical Hollow Magnetic Microrobot: The main drawback of using MJRs based on Pt/H_2O_2 relies on their biocompatibility issues for future biomedical applications. Different researches investigate biocompatible micro/nanorobots [10]. Among proposed designs, MJR based on a Janus hollow particle powered by biologically available urea is a promising solution. To validate the proposed model, this paper considers the Janus hollow magnetic particle developed by Ma et al. [10]. Their MJRs are based on Janus hollow mesoporous particle covered with enzyme urease to trigger the bio-catalytic decomposition of urea into CO_2 and NH_3. The MJR can be coated with Fe(10 nm)/Au(3 nm) for external magnetic control. However, details of the self-phoretic motion is not fully addressed at present, and the swimming velocity (15) should be further investigated. The parameter

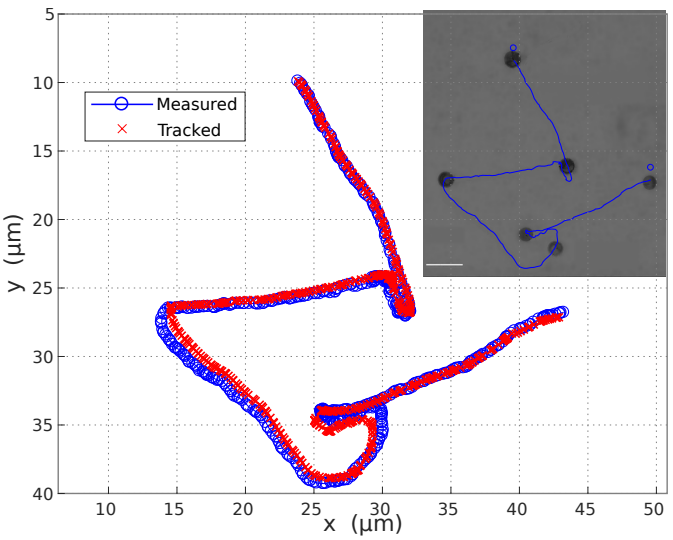

Fig. 8. Measured and tracked path of a spherical hollow MJR using SDC-DKF, from experimental data carried by Ma et al. [10].

set considered is reported in the Table I.b.

SDC-DKF is employed to estimate $\hat{\mathbf{x}}$ and $\hat{\mathbf{u}}$, from MJR's observations $\mathbf{y}$ provided in experiments realized by Ma et al. [10]. The measured and the tracked path is shown in Fig. 8. Once again, the SDC-DKF follows properly the observed path. Fig. 9 presents the error between the measured output $\mathbf{y}$ and its estimates $\hat{\mathbf{y}}$. The error statistics are $\text{RMSE}(x) = 1.10\,\mu\text{m}$, $\text{RMSE}(y) = 1.11\,\mu\text{m}$ and $\text{RMSE}(\theta) = 2.35\,\text{deg}$. Fig. 10 shows the input estimation $\hat{\mathbf{u}}$. The estimated swimming velocity has a mean value of $\langle u_0 \rangle = 9.75\,\mu\text{m/s}$ and $\text{RMSE}(u_0) = 10.06\,\mu\text{m/s}$, that are consistent with the velocity of about $10\,\mu\text{m/s}$ given by Ma et al. [10]. These results also validate the consistency of the proposed approach to describe the behavior of MJR, while accessing to the uncontrollable inputs. Nevertheless, the estimations have, here, a slightly larger discrepancy than the previous case. This is reasonably due to: i) a divergence in the spherical shape of the hollow particle with its surface coated with enzyme urease; ii) some difficulty to measure properly the orientation, θ, of the MJR; and iii) a decrease of the particle's size and an increase of its dynamics.

C. Discussion

When the MJR's direction θ changes significantly the estimation errors increase. This is asserted with the appearance of some significant peaks in the position estimation error (e.g. at times $t_a..t_c$ in Fig. 6). Further investigation assumes that a poor measure θ or estimate $\hat{\theta}$ also degrade significantly estimation of the magnetic field. Consequently, the estimation errors tend to be accumulated. SDC-DKF then requires a good knowledge of orientation θ to provide correct state and unknown input estimations of MJR. This dependence is related to the fact that θ is a state-dependent term necessary for the evaluation of the input matrix $\mathbf{B}(\mathbf{x})$.

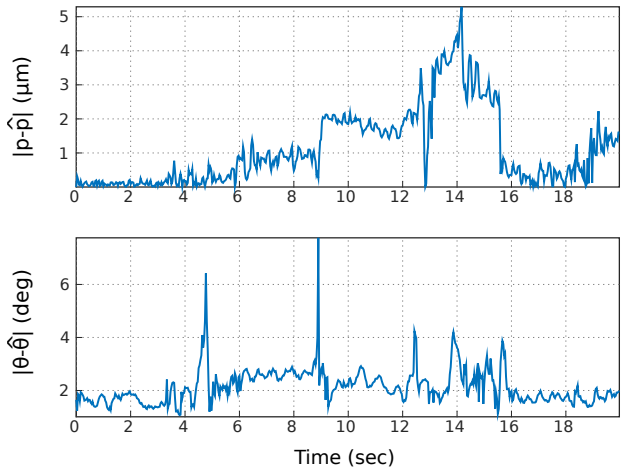

Fig. 9. The estimation error of the position ($|\mathbf{p}-\hat{\mathbf{p}}|$, with $\mathbf{p}=(x,y)$), and of the orientation, $|\theta-\hat{\theta}|$, of the spherical hollow MJR.

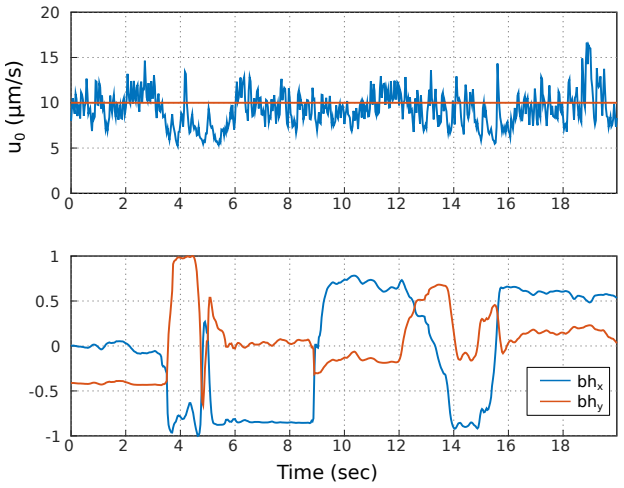

Fig. 10. The estimated input $\hat{\mathbf{u}} = (u_0, \beta b_x, \beta b_y)$ from the observed experimental data. (top) The red-line shows the mean thrust velocity of $u_0 \approx 10\,\mu\text{m/s}$ reported by Ma et al. [10]. (bottom) normalized value of the actuated field βb_x and βb_y.

IV. CONCLUSION

In this study, we demonstrated that the behavior of magnetic Janus catalytic microrobot can be estimated through an SDC-DKF even if the inputs are unknown. We find that there is good agreement between the estimations computed from our theoretical predictions and the experimental observations in a wide range of model parameter variations. The proposed MJR modeling offers an analytic description that opens the way to explicit and more advanced control strategies. Similarly, the SDC-DKF is a first attempt to combine SDC parameterization with a common DKF methodology. Indeed, there is a strong analogy between the DKF dealing with uncontrollable inputs and with those for parameters estimation. In this paper favored to deal with the uncontrollable inputs problem. Obviously, a combined problem of estimating state-input-parameters can also be defined. Further extents could then be envisioned. For instance, the proposed MJR's model can be extended to different micro/nanomotors such as nanorod or conical microjet by adapting the swimming velocity (6), and the hydrodynamics (7)-(8) analytical expressions. However, the dynamic model expression should be even more non-linear, and the proposed SDC-DKF further extended. Actually, despite some robustness against design parameters is observed with the SDC-DKF, its efficiency is strongly sensitive to the good knowledge of the state. Up to now very few works have investigated the medical imaging of MJR, and more generally the medical imaging of micro/nano-robot that remains an open issue that should be further investigated. In particular, the determination of the orientation of spherical MJR is a challenging problem. Finally, in the considered experiments the Brownian diffusion remains globally low. This associated with inputs that can not always be assumed as Gaussian stochastic processes, more advanced and robust stochastic filtering should be envisaged.

APPENDIX

The state dependent coefficient dual Kalman filter (SDC-DKF) algorithm goes as follows:

- First prediction stage for the a priori state

$$\breve{\mathbf{x}}_{k|k-1} = \mathbf{A}_{k-1}\hat{\mathbf{x}}_{k-1|k-1} \tag{25}$$

- Prediction stage for the a priori input

$$\hat{\mathbf{u}}_{k|k-1} = \hat{\mathbf{u}}_{k-1|k-1} \tag{26}$$

$$^{u}\mathbf{P}_{k|k-1} = {}^{u}\mathbf{P}_{k-1|k-1} + {}^{u}\mathbf{Q} \tag{27}$$

- Update stage for the input
  - Calculation of Kalman gain for input:

$$^{\mathbf{u}}\mathbf{K}_k = {}^{\mathbf{u}}\mathbf{P}_{k|k-1}\mathbf{D}_{k-1}^T\left(\mathbf{D}_{k-1}{}^{u}\mathbf{P}_{k|k-1}\mathbf{D}_{k-1}^T + {}^{\mathbf{u}}\mathbf{R}\right)^{-1}, \tag{28}$$

  - Correction of predictions of a posteriori input estimate

$$\hat{\mathbf{u}}_{k|k} = \hat{\mathbf{u}}_{k|k-1} + {}^{u}\mathbf{K}_k\left(\mathbf{y}_k - \mathbf{C}_{k-1}\breve{\mathbf{x}}_{k|k-1} - \mathbf{D}_{k-1}\hat{\mathbf{u}}_{k|k-1}\right) \tag{29}$$

$$^{u}\mathbf{P}_{k|k} = {}^{u}\mathbf{P}_{k|k-1} - {}^{u}\mathbf{K}_k\mathbf{D}_{k-1}{}^{\mathbf{u}}\mathbf{P}_{k|k-1} \tag{30}$$

- Prediction stage for the state with the estimate input

$$\hat{\mathbf{x}}_{k|k-1} = \breve{\mathbf{x}}_{k|k-1} + \mathbf{B}_{k-1}\hat{\mathbf{u}}_{k|k} \tag{31}$$

$$^{x}\mathbf{P}_{k|k-1} = \mathbf{A}_{k-1}{}^{x}\mathbf{P}_{k-1|k-1}\mathbf{A}_{k-1}^T + {}^{x}\mathbf{Q} \tag{32}$$

- Update stage for the state
  - Calculation of Kalman gain for state:

$$^{x}\mathbf{K}_k = {}^{\mathbf{x}}\mathbf{P}_{k|k-1}\mathbf{C}_{k-1}^T\left(\mathbf{C}_{k-1}{}^{\mathbf{x}}\mathbf{P}_{k|k-1}\mathbf{C}_{k-1}^T + {}^{x}\mathbf{R}\right)^{-1} \tag{33}$$

  - Correction of predictions of a posteriori state estimate

$$\hat{\mathbf{x}}_{k|k} = \hat{\mathbf{x}}_{k|k-1} + {}^{x}\mathbf{K}_k\left(\mathbf{y}_k - \mathbf{C}_{k-1}\hat{\mathbf{x}}_{k|k-1} - \mathbf{D}_{k-1}\hat{\mathbf{u}}_{k|k-1}\right) \tag{34}$$

$$^{x}\mathbf{P}_{k|k} = {}^{x}\mathbf{P}_{k|k-1} - {}^{x}\mathbf{K}_k\mathbf{C}_{k-1}{}^{u}\mathbf{P}_{k|k-1} \tag{35}$$

REFERENCES

[1] J. Katuri, X. Ma, M. M. Stanton, and S. Sanchez, "Designing micro-and nanoswimmers for specific applications," *Accounts of chemical research*, vol. 50, no. 1, pp. 2–11, 2017.

[2] W. Gao, X. Feng, A. Pei, Y. Gu, J. Li, and J. Wang, "Seawater-driven magnesium based janus micromotors for environmental remediation," *Nanoscale*, vol. 5, no. 11, pp. 4696–4700, 2013.

[3] J. Li, B. E.-F. de Ávila, W. Gao, L. Zhang, and J. Wang, "Micro/nanorobots for biomedicine: Delivery, surgery, sensing, and detoxification," *Science Robotics*, vol. 2, no. 4, 2017.

[4] J. R. Howse, R. A. Jones, A. J. Ryan, T. Gough, R. Vafabakhsh, and R. Golestanian, "Self-motile colloidal particles: from directed propulsion to random walk," *Phys. review letters*, vol. 99, no. 4, p. 048102, 2007.

[5] L. Baraban, D. Makarov, R. Streubel, I. Monch, D. Grimm, S. Sanchez, and O. G. Schmidt, "Catalytic janus motors on microfluidic chip: deterministic motion for targeted cargo delivery," *ACS Nano*, vol. 6, no. 4, pp. 3383–3389, 2012.

[6] I. S. Khalil, V. Magdanz, S. Sanchez, O. G. Schmidt, and S. Misra, "Precise localization and control of catalytic janus micromotors using weak magnetic fields," *Int. J. of Adv. Robotic Systems*, vol. 12, no. 1, p. 2, 2015.

[7] R. Golestanian, T. Liverpool, and A. Ajdari, "Designing phoretic micro-and nano-swimmers," *New J. of Phys.*, vol. 9, no. 5, p. 126, 2007.

[8] S. Wang and N. Wu, "Selecting the swimming mechanisms of colloidal particles: Bubble propulsion versus self-diffusiophoresis," *Langmuir*, vol. 30, no. 12, pp. 3477–3486, 2014.

[9] J. Li, O. E. Shklyaev, T. Li, W. Liu, H. Shum, I. Rozen, A. C. Balazs, and J. Wang, "Self-propelled nanomotors autonomously seek and repair cracks," *Nano Letters*, vol. 15, no. 10, pp. 7077–7085, 2015.

[10] X. Ma, X. Wang, K. Hahn, and S. Sanchez, "Motion control of urea-powered biocompatible hollow microcapsules," *ACS Nano*, vol. 10, no. 3, pp. 3597–3605, 2016.

[11] T. Li, X. Chang, Z. Wu, J. Li, G. Shao, X. Deng, J. Qiu, B. Guo, G. Zhang, Q. He, L. Li, and J. Wang, "Autonomous collision-free navigation of microvehicles in complex and dynamically changing environments," *ACS Nano*, vol. 11, no. 9, pp. 9268–9275, 2017.

[12] S. Das, E. B. Steager, K. J. Stebe, and V. Kumar, "Simultaneous control of spherical microrobots using catalytic and magnetic actuation," in *MARSS*. IEEE, 2017, pp. 1–6.

[13] S. Das, E. B. Steager, M. A. Hsieh, K. J. Stebe, and V. Kumar, "Experiments and open-loop control of multiple catalytic microrobots," *Journal of Micro-Bio Robotics*, vol. 14, no. 1, pp. 25–34, Jun. 2018.

[14] J. J. Abbott, O. Ergeneman, M. P. Kummer, A. M. Hirt, and B. J. Nelson, "Modeling magnetic torque and force for controlled manipulation of soft-magnetic bodies," *IEEE Trans. Robot.*, vol. 23, no. 6, pp. 1247–1252, 2007.

[15] K. E. Peyer, L. Zhang, and B. J. Nelson, "Bio-inspired magnetic swimming microrobots for biomedical applications," *Nanoscale*, vol. 5, no. 4, pp. 1259–1272, 2013.

[16] I. S. Khalil, V. Magdanz, S. Sanchez, O. G. Schmidt, and S. Misra, "3-d closed-loop control of self-propelled microjets," *Appl. Phy. Letters*, vol. 103, no. 172404, pp. 1–4, 2013.

[17] T. Mano, J.-B. Delfau, J. Iwasawa, and M. Sano, "Optimal run-and-tumble-based transportation of a janus particle with active steering," *PNAS*, vol. 14, pp. E2580–E2589, 2017.

[18] L. W. Rogowski, X. Zhang, L. Huang, A. Bhattacharjee, J. S. Lee, A. T. Becker, and M. J. Kim, "Feedback control and 3d motion of heterogeneous janus particles," in *Int. Conf. on Rob. and Autom.* IEEE, 2019, pp. 1352–1357.

[19] L. Huang, J. Leclerc, and A. T. Becker, "Analysis of 3d position control for a multi-agent system of self-propelled agents steered by a shared, global control input," in *Int. Conf. on Rob. and Autom.* IEEE, 2019, pp. 1352–1357.

[20] U. K. Cheang, H. Kim, D. Milutinovic, J. Choi, and M. J. Kim, "Feedback control of an achiral robotic microswimmer," *Journal of Bionic Engineering*, vol. 14, pp. 245–259, 2017.

[21] M. Hou and P. Muller, "Design of observers for linear systems with unknown inputs," *IEEE Trans. Autom. Control*, vol. 37, no. 6, pp. 871–875, 1992.

[22] N. J. Gordon, D. J. Salmond, and A. F. Smith, "Novel approach to nonlinear/non-gaussian bayesian state estimation," in *IEE Radar and Signal Processing)*, vol. 140, no. 2. IET, 1993, pp. 107–113.

[23] C.-S. Hsieh, "Robust two-stage kalman filters for systems with unknown inputs," *IEEE Trans. Autom. Control*, vol. 45, no. 12, pp. 2374–2378, 2000.

[24] S. Gillijns and B. De Moor, "Unbiased minimum-variance input and state estimation for linear discrete-time systems," *Automatica*, vol. 43, pp. 111–116, 2007.

[25] E. Lourens, E. Reynders, G. De Roeck, G. Degrande, and G. Lombaert, "An augmented kalman filter for force identification in structural dynamics," *Mechanical Systems and Signal Processing*, vol. 27, pp. 446–460, 2012.

[26] S. E. Azam, E. Chatzi, C. Papadimitriou, and A. Smyth, "Experimental validation of the dual kalman filter for online and real-time state and input estimation," in *Model Validation and Uncertainty*, 2015, vol. 3, pp. 1–13.

[27] J. L. Anderson, "Colloid transport by interfacial forces," *An. rev. of Fluid Mechanics*, vol. 21, no. 1, pp. 61–99, 1989.

[28] Y. Solomentsev and J. L. Anderson, "Electrophoresis of slender particles," *J. of Fluid Mechanics*, vol. 279, pp. 197–215, 1994.

[29] S. Sanchez, A. A. Solovev, S. Schulze, and O. G. Schmidt, "Controlled manipulation of multiple cells using catalytic microbots," *Chemical Communications*, vol. 47, no. 2, pp. 698–700, 2011.

[30] H. Banks, B. Lewis, and H. Tran, "Nonlinear feedback controllers and compensators: a state-dependent Riccati equation approach," *Comput. Opti. and Applications*, vol. 37, no. 2, pp. 177–218, 2007.

[31] M. NøRgaard, N. K. Poulsen, and O. Ravn, "New developments in state estimation for nonlinear systems," *Automatica*, vol. 36, no. 11, pp. 1627–1638, 2000.

[32] C. P. Mracek, J. Clontier, and C. A. D'Souza, "A new technique for nonlinear estimation," in *IEEE Int. Conf. on Contr. Appl.*, 1996, pp. 338–343.

[33] D. A. Haessig and B. Friedland, "State dependent differential riccati equation for nonlinear estimation and control," *IFAC*, vol. 35, pp. 405–410, 2002.